Accuracy Assessment of User Micromobility Models for THz Cellular Systems

N. Stepanov, A. Turlikov
State University of Aerospace Instrumentation (SUAI University), St-Petersburg, Russia

V. Begishev
Peoples' Friendship University of Russia (RUDN University), Moscow, Russia

D. Moltchanov, Y. Koucheryavy
Tampere University, Finland

ABSTRACT

Terahertz (THz, 0.3 – 3 THz) communications are envisioned as one of the enablers at the air interface for sixth-generation (6G) cellular systems. However, by utilizing large antenna arrays to overcome severe path losses, this system will suffer from micromobility phenomenon manifesting itself in occasional rotations and displacements of user equipment (UE) in the hand of a user. In this paper, based on the measurements of micromobility patterns we propose several models characterized by various degrees of details to capture micromobility patterns of different applications. By utilizing the time to the outage as a metric we compare their accuracy. Our results show that drift to the origin is a critical property that has to be captured by the model. While the two-dimensional Markov model is shown to provide the most accurate approximation, the decomposed Brownian motion model is characterized by the worst match of data. The decomposed one-dimensional Markov model provides the trade-off between simplicity and approximation accuracy.

CCS CONCEPTS

• **Networks** → **Mobile networks**; *Network measurement*;

The research of A. Turlikov and N. Stepanov was prepared with the financial support of the Ministry of Science and Higher Education and of the Russian Federation, grant agreement No. FSRF-2020-0004, "Scientific basis for architectures and communication systems development of the onboard information and computer systems new generation in aviation, space systems and unmanned vehicles".

mmNets 2021, January 31-February 4, 2022, New Orleans, LA, USA

ACM ISBN 978-1-4503-8699-9/22/01…$15.00
https://doi.org/10.1145/3477081.3481676

ACM Reference Format:
N. Stepanov, A. Turlikov, V. Begishev, and D. Moltchanov, Y. Koucheryavy. 2022. Accuracy Assessment of User Micromobility Models for THz Cellular Systems. In *5th ACM Workshop on Millimeter-Wave and Terahertz Networks and Sensing Systems (mmNets 2021), January 31-February 4, 2022, New Orleans, LA, USA.* ACM, New York, NY, USA, 6 pages. https://doi.org/10.1145/3477081.3481676

1 INTRODUCTION

Terahertz (THz, 0.3 – 3 THz) communications systems are envisioned to become a new radio access technology (RAT) in prospective sixth-generation (6G) cellular networks [13, 18]. By potentially utilizing tens of gigahertz of consecutive bandwidth this RAT may enable rate greedy applications at the air interface at massive scales including virtual reality (VR), holographic communications, remote monitoring, etc.

To overcome severe path losses, THz systems are expected to utilize massive antenna arrays at least at the base station (BS) side [1]. These antennas will have extremely directional radiation patterns having half-power beamwidth (HPBW) on the order of degree or even fraction of a degree [4]. As a result in addition to blockage impairments that are already significant at the lower millimeter wave (mmWave) band, these systems will be susceptible to UE micromobility, i.e., fast rotations and displacements in hands of a user. Depending on the application type, this phenomenon may lead to frequent outages invoking beamalignment procedure.

The impact of multiconnectivity on THz link performance has been addressed in [11, 12]. These studies have shown that depending on the type of applications utilizing THz channel, conventional periodic beamalignment system design utilized in 5G systems may lead to drastic performance degradation in terms of achievable link rate and outage probability due to frequent misalignments caused by micromobility. The on-demand beamalignment is much more efficient for applications characterized by high micromobility but, at the same time, always induces outage situations and are not in line with the current cellular systems design. This implies that the beamtracking schemes utilized in prospective THz communications should not be static in nature requiring dynamic adaptation to both dynamically changing multi-path

channel conditions and the type of application utilizing the resources of the air interface. However, the model utilized in [12] is based on unbiased Brownian motion that may not capture the details of micromobility of realistic applications.

Motivated by the lack of micromobility models, the aim of this paper is to compare evaluate the accuracy of micromobility models for THz communications. To this aim, we first carry out a measurements campaign of UE micromobility for different applications. We then identify critical properties of these patterns and propose three models characterized by different degrees of details taken into account and complexity, including two-dimensional Markov chain, simple unbiased Brownian motion, and decomposed one-dimensional Markov model with distance-dependent drift and velocity. We compare these models with statistical data based on the main metric of interest – time to an outage.

The rest of the paper is organized as follows. In Section 2 we introduce the considered scenario and also describe the measurement methodology. Further, in Section 3 we perform statistical analysis of obtained data. Micromobility models are introduced in Section 4 while their comparison is presented in Section 5. Conclusions are drawn in the last section.

2 SYSTEM MODEL AND METHODOLOGY

In this paper, we consider a point-to-point communications link between THz BS and UE. Both THz BS and UE are equipped with identical planar two-dimensional antenna arrays with $N_B \times N_B$ and $N_U \times N_U$ elements each. We assume a cone antenna radiation pattern [10], with non-zero gain over the main lobe's HPBW approximated by $102^\circ/N_B$ and $102^\circ/N_U$ [3]. The THz BS is assumed to be tightly fixed. Contrarily, THz UE is subject to micromobility affecting beam alignment between UE and BS.

In this paper, we concentrate on such distances between BS and UE, d, that there is no outage when main lobes of UE and BS antennas are oriented towards each other. This distance can be estimated for a given carrier frequency f_C by utilizing THz specific propagation model specified theoretically in, e.g., [2, 5] or recently via measurements in [16, 17].In these conditions, by utilizing geometric interpretation of the considered link model illustrated in Fig. 1 we observe that the system enters the outage state when the center of the UE beam leaves the squared shaped area corresponding to HPBW of THz BS. Observe that it could happen due to small displacements of UE over Ox and Ox axes as well as due to yaw (vertical axis) and pitch (transverse axis) motions of UE in the user's hands. Observe that small displacements over Oz axis as well as roll (longitudinal axis) motion do not severely affect the communications. Thus, to exhaustively capture UE micromobility affecting THz communications it is sufficient to characterize the motion pattern of the center of UE beam. We now proceed by describing the associated methodology and the beam detection principle.

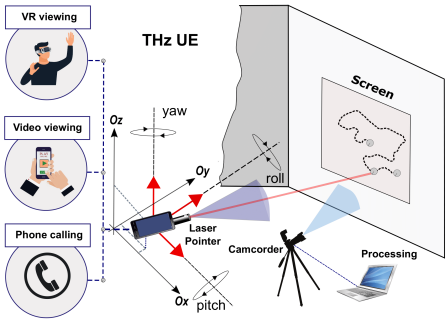

Figure 1: THz micromobility measurements setup.

Instead of relying upon smartphone's motion sensors that are characterized by excessive errors, we use the direct measurements methodology, see Fig. 1. Particularly, we track the movement of the center of UE HPBW. To facilitate it, it is sufficient to utilize a laser pointer firmly connected with the smartphone. To track the laser spot we utilize a Nikon D3100 camera in the video recording mode at a resolution of 1280x720, 30 frames-per-second. Laser pointer with laser diameter of 3 mm, output power of 5 mW, and light wavelength of 650 nm±10 has been utilized. A tripod has been used to mount the camera capturing the motion of the laser pointer representing the center of THz beam's HPBW. A laser pointer is firmly mounted on a mobile device and shines on the flat wall surface. The distance between the wall and the camera was set to 2 m. The observed area on the wall is 1.5×1.5 m. We consider three typical applications: (i) video viewing, (ii) phone calling, (iii) VR viewing.

To obtain the statistical data 30 independent experiments have been carried out for each considered application. The duration of each experiment has been set to 10 s. To obtain the laser trajectory out of video recordings the background difference method has been utilized [9].

2.1 Metrics of Interest

As the main metric of interest for comparison of micromobility models we utilize the uninterrupted time in connected state. This is defined as the interval between time instant, when UE and BS antennas are perfectly aligned (e.g., as a result of beamalignment procedure) till the center of UE HPBW touches the squared boundary. Note that in the context of the stochastic model it is interpreted as first passage time (FPT) to the square boundary.

3 STATISTICAL ANALYSIS

3.1 Statistical Analysis

Sample trajectories of considered applications are illustrated in Fig. 2. Visual observation of the presented data allows to

conclude that considered applications are characterized by different ranges of values. Particularly, VR viewing application is characterized by the higher dispersion from the origin while the corresponding ranges for video viewing and phone call applications are much smaller.

From the modeling perspective, we have the following requirements for potential stochastic processes representing micromobility patterns. As demonstrated in [12], in order to evaluate outage probability and spectral efficiency one needs to obtain the distribution of FPT to the beam boundary. However, obtaining FPT distribution when utilizing two-dimensional random walk models is much more complicated as compared to one-dimensional ones [8, 14].

The dimension reduction can be achieved by utilizing special properties of micromobility patterns. Particularly, if there is a radial symmetry in the micromobility characteristics it would imply that one may restrict its characterization to a one-dimensional random walk. Visual observation of sample trajectories presented in Fig. 2 however does not allow to confirm this hypothesis. Furthermore, the Kolmogorov-Smirnov test for heterogeneity of samples performed pairwise of trajectories belonging to different quadrants of Cartesian coordinates with the level of significance show that the corresponding probability mass functions (pmf) are quantitatively different even under the loose level of significance set to $\alpha = 0.1$.

Another way to simplify the modeling of micromobility patterns is to decompose the two-dimensional motions into two components corresponding to Ox and Oy axes. In this case, the overall FPT to the outage can be obtained as the minimum of FPTs of two processes. However, the inherent difficulty with this approach is that individual motions might be dependent and this dependence has to be accounted for in FPT calculations. To assess the level of dependence Fig. 3 presents the coefficient of correlation between absolute displacements along x- and y-coordinates of individual mobility processes for all considered applications as a function of time resolution Δt. Analyzing the presented data, one may

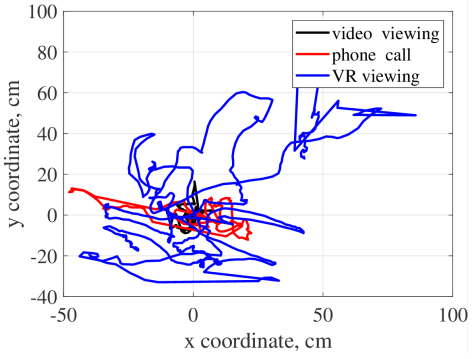

Figure 2: Sample trajectories of applications.

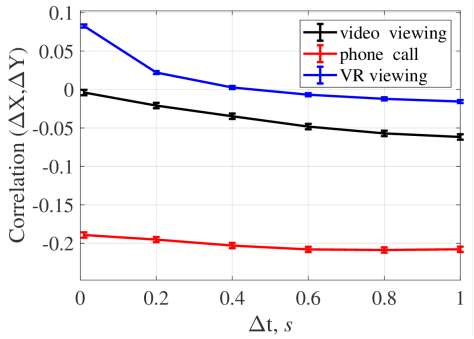

Figure 3: Correlation between x- and y-axes.

observe that individual processes for video and VR viewing applications are completely uncorrelated. The correlation coefficient for phone call application for all considered values of time resolution is limited by -0.2. These observations allow us to deduce that for the set of considered applications individual processes can be considered uncorrelated.

Having revealed the absence of correlation between individual components of decomposed mobility patterns, we now proceed with illustrating two critical characteristics of individual processes, drift from the origin and mean velocity in Fig. 4 and Fig. 5, respectively. The former metric represents the probability of moving from the center as a function of the distance while the latter is the estimate of distance-dependent velocity. Observing the presented data, one may deduce that expectedly, all mobility patterns are characterized by significant drift from the origin. In fact, the probability of moving from the center coincides for all considered patterns at around 0.17 and is independent of the distance from the origin. The velocity data are clearly both application and axis dependent but still can be assumed to be independent from the distance.

4 MICROMOBILITY MODELS

4.1 Brownian Motion Model

Following [12], we represent movement over x- and y-axes by independent Brownian motions. Recall, that Brownian motion process is described by [14]

$$\frac{\partial c(x,t)}{\partial t} - D\frac{\partial^2 c(x,t)}{\partial x} = 0, \quad t > 0, \tag{1}$$

where the "concentration" $c(x,t)$ is interpreted as the probability density of having a diffusing point at a certain coordinate at time t, D is the diffusion coefficient.

The only two parameters required to represent micromobility patterns are D_x and D_y – diffusion constants over Ox and Oy axes. These can be estimated from the statistical data.

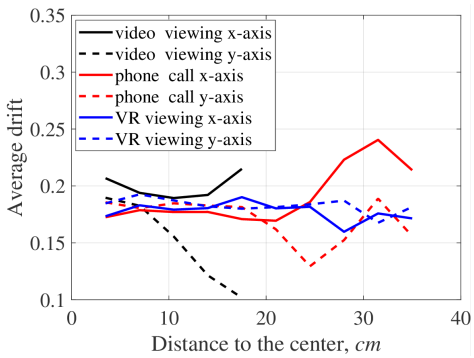

Figure 4: Drift from the origin over x- and y-axes.

Once parameterized, the sought probability density function (pdf) of FPT can be determined as follows

$$f_{T_{X,Y}}(t) = f_X(t)[1 - F_Y(t)] + f_Y(t)[1 - F_X(t)], \quad (2)$$

where $f_X(t)$ and $f_Y(t)$ are pdf of FPT over Ox and Oy axe, respectively, while $F_Y(t)$ and $F_Y(t)$ are the corresponding cumulative distribution functions (CDF). The former coincide with the pdf of FPT time with absorbing boundary at M and reflecting boundary as 0 and are both provided by [6]

$$f_\cdot(t) = \frac{M}{\sqrt{4\pi D t^3}} \exp\left(-\frac{M^2}{4Dt}\right), \; t > 0, \quad (3)$$

where $2M$ is the length of the square.

Note that (2) assumes that movements along Ox and Oy axes are independent. Furthermore, observe that this model does not take into account both drift to the origin and distant-dependent velocity.

4.2 Two-Dimensional Markov chain

Consider now the two-dimensional Markov model. This model is obtained by inducing a regular grid and associating each state of the model with a cell. To parameterize this model, we need to determine the number of states, $N \times N$, corresponding to the grid size, and estimate the transition

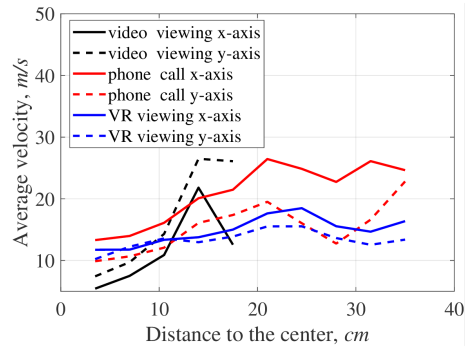

Figure 5: Velocity characteristics over x- and y-axes.

probabilities p_{ij}, $i, j = 1, 2, \ldots, N^2$. There is a critical parameter that affects the choice of the number of states – spatial resolutions of the model, Δs. The choice of Δs affects the trade-off between the amount of available statistics and the model accuracy. For the model to accurately predict FPT Δs has to be at least five times smaller than half of HPBW at the considered distance d [8, 14]. For typical THz communication distances (up to 50 m) and modern antenna arrays of up to 128×128 elements one is interested in radii of at least 10 cm and no more than 50 cm [11]. Thus, in what follows we will use $\Delta s = 2$ cm to cover the screen space of 1.5×1.5 m resulting in $N^2 = 5625$. To keep the balance between state transitions as a time resolution of the model we utilize the native one, $\Delta t = 1/30$ s, to recover lost waypoints.

Once N^2 is determined, we obtain the transition probabilities p_{ij}, $i, j = 1, 2, \ldots, N^2$ by using the conventional methodology. We first define the state boundaries and then calculate the number of state changes for the particular values of i and j between the previous and the current value in the trace. Finally, we divide it by the number of samples in the trace.

As compared to the Brownian motion model, the two-dimensional Markov model implicitly account for potential correlation between movements along Ox and Oy axes as well as drift to the origin and distant-dependent velocity. However, even though the pmf of the FPT can be found numerically by formulating and solving the set of linear equations [15] the state space of the resulting model prohibits its efficient applications in performance evaluation studies.

4.3 One-Dimensional Markov Model

A simple Brownian motion model allows for analytical analysis of THz communications as illustrated in [12] but may fail to capture intrinsic properties of micromobility patterns. In contrast, the two-dimensional Markov model implicitly accounts for them but is characterized by the extreme state-space preventing its use in analytical performance studies.

As an alternative, we drop the dependence between movements along Ox and Oy axes by modeling movements along Ox and Oy axes by individual Markov chains. The transition probabilities for these chains are estimated by utilizing the methodology described above for two-dimensional Markov model. Particularly, we utilize the same spatial and temporal resolutions of $\Delta s = 2$ cm $\Delta t = 1/30$ s. In our case the number of states of each components is just 75.

Note that this model still captures potential drift to the origin and distance-dependent velocity over individual axes. Furthermore, having a limited number of states a direct numerical calculation is still feasible. Finally, as one may observe some of the considered applications are characterized by nearly constant drift to the origin and velocity. This potentially enables to consider a specific class of one-dimensional

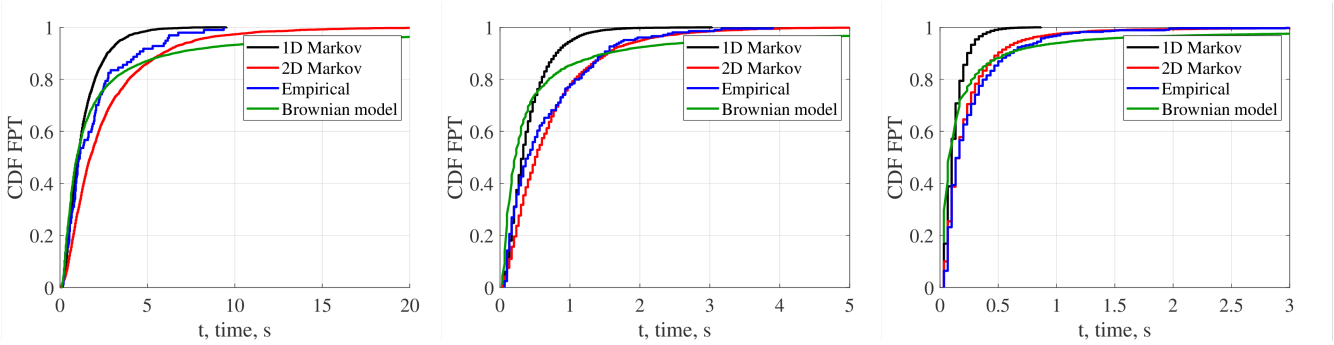

(a) Video viewing (b) Phone call (c) VR viewing

Figure 6: Illustration of empirical and modeled FPT CDFs for considered applications.

Markov chains – birth-death processes with constant transition probabilities. For these models, explicit expressions for FPT times can be obtained by utilizing fundamental matrix theory [7]. For this to be feasible, one also need to decrease the spatial resolution of the model Δs further ensuring that transitions to nearby states are only feasible. However, further exposition of this topic is out of the scope of this paper.

5 NUMERICAL RESULTS

In this section we provide a comparison between considered models. The main metric of interest is the uninterrupted connectivity time characterized by FPT of the considered models. We consider both CDFs and mean values for comparison.

We start with Fig. 6 showing FPT CDFs of considered models as well as empirical CDF for all considered applications and 4 cm circular boundary representing HPBW projection. Visual observation indicates that the Brownian motion model provides the worst approximation as it significantly deviates from the empirical CDF for both small and large values of FTP times. Recalling statistical characteristics of the mobility patterns, the reasons for mismatch can be mainly attributed to the inability of this model to capture drift to the origin and the lack of dependence between axial movements. To this end, as one may observe, two-dimensional Markov model provides a tighter approximation for empirical CDF as both abovementioned properties are implicitly captured. Finally, the decomposed one-dimensional Markov chain provides a better match of the empirical CDF as compared to the Brownian motion model. The rationale is that in spite of its decomposed structure, it still captures the drift to the origin property of micromobility patterns.

Consider now the behavior of models in detail for VR application, one-dimensional Markov model and different HPBW projection radii, 4, 6, and 8 cm. As one may observe, the model is characterized by different behavior for different radii. The biggest mismatch is observed for 4 cm. Then, at 6 cm the match is better except for the tail behavior. Finally, at the maximum considered radii, 8 cm, the tail is closely approximated while the mismatch is observed for small values of FPTs. This behavior indicates that the accuracy of the considered model heavily depends on both antenna configuration and communications distance between BS and UE as these parameters directly translate to HPBW projection.

Now, we proceed with the mean values of FPT time for considered applications and models as illustrated in Fig. 8 as a function of radii representing HPBW projection. Note that for video viewing application the amount of statistics is insufficient to reliably calculate the mean value for boundary lengths larger than 6 cm. Expectedly, the best approximation is observed for the 2D Markov model as it captures all the statistical characteristics of the considered mobility patterns. However, surprisingly, both decomposed Brownian motion and one-dimensional Markov model provide qualitatively similar approximation for the mean FPT values.

6 CONCLUSIONS

Along with blockage of propagation paths, micromobility of UE in hands of users is considered to provide a significant

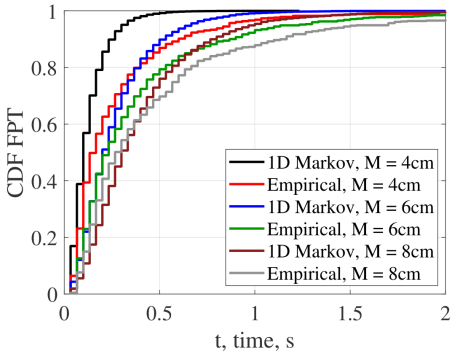

Figure 7: FPT CDFs for VR and different radii.

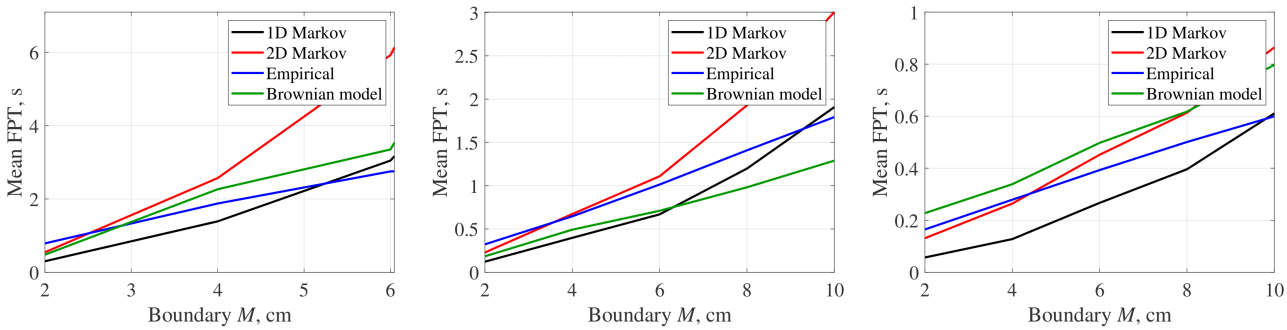

(a) Video viewing (b) Phone call (c) VR viewing

Figure 8: Illustration of empirical and modeled mean FPT values for considered applications.

impact on future THz cellular systems. In this paper, based on the measurements campaign, we formalized three micro-mobility models having different degrees of details including simple unbiased Brownian motion, two-dimensional Markov chain and decomposed one-dimensional Markov model.

Our numerical results illustrate that for considered applications dependence between axial movements is insignificant while the velocity remains relatively intact with the distance. At the same time, drift to the origin is non-negligible. These properties allow reducing the model dimension that significantly simplifies the use of the models in performance evaluation studies. Our results indicate that the most complex directly fitted two-dimensional Markov chain model provides the best approximation in terms of both CDF and mean values of the time to the outage. The decomposed Brownian motion model fails to accurately capture distributional properties of the time to the outage. For practical applications, the one-dimensional decomposed Markov chain model provides a viable compromise between simplicity and accuracy.

REFERENCES

[1] Ian F Akyildiz and Josep Miquel Jornet. 2016. Realizing ultra-massive MIMO (1024× 1024) communication in the (0.06–10) terahertz band. *Nano Communication Networks* 8 (2016), 46–54.

[2] Pavel Boronin, Vitaly Petrov, Dmitri Moltchanov, Yevgeni Koucheryavy, and Josep Miquel Jornet. 2014. Capacity and throughput analysis of nanoscale machine communication through transparency windows in the terahertz band. *Nano Communication Networks* 5, 3 (2014), 72–82.

[3] A Balanis Constantine et al. 2005. Antenna theory: analysis and design. *Microstrip Antennas, John Wiley & Sons* (2005).

[4] Alice Faisal, Hadi Sarieddeen, Hayssam Dahrouj, Tareq Y Al-Naffouri, and Mohamed-Slim Alouini. 2020. Ultramassive MIMO Systems at Terahertz Bands: Prospects and Challenges. *IEEE Vehicular Technology Magazine* 15, 4 (2020), 33–42.

[5] Josep Miquel Jornet and Ian F Akyildiz. 2011. Channel modeling and capacity analysis for electromagnetic wireless nanonetworks in the terahertz band. *IEEE Transactions on Wireless Communications* 10, 10 (2011), 3211–3221.

[6] Samuel Karlin. 2014. *A first course in stochastic processes*. Academic press.

[7] John G Kemeny, James Laurie Snell, et al. 1960. *Finite markov chains*. Vol. 356. van Nostrand Princeton, NJ.

[8] Pavel L Krapivsky, Sidney Redner, and Eli Ben-Naim. 2010. *A kinetic view of statistical physics*. Cambridge University Press.

[9] Yaxin Liu, Yanqiang Zhang, Yufeng Yao, and Ming Zhong. 2018. Laser Point Detection Based on Improved Target Matching Method for Application in Home Environment Human-Robot Interaction. In *2018 11th International Workshop on Human Friendly Robotics (HFR)*. IEEE, 13–18.

[10] Vitaly Petrov, Mikhail Komarov, Dmitri Moltchanov, Josep Miquel Jornet, and Yevgeni Koucheryavy. 2017. Interference and SINR in millimeter wave and terahertz communication systems with blocking and directional antennas. *IEEE Transactions on Wireless Communications* 16, 3 (2017), 1791–1808.

[11] Vitaly Petrov, Dmitri Moltchanov, Yevgeni Koucheryavy, and Josep M Jornet. 2018. The effect of small-scale mobility on terahertz band communications. In *Proceedings of the 5th ACM International Conference on Nanoscale Computing and Communication*. 1–2.

[12] Vitaly Petrov, Dmitri Moltchanov, Yevgeni Koucheryavy, and Josep Miquel Jornet. 2020. Capacity and Outage of Terahertz Communications with User Micro-mobility and Beam Misalignment. *IEEE Transactions on Vehicular Technology* (2020).

[13] Michele Polese, Josep Miquel Jornet, Tommaso Melodia, and Michele Zorzi. 2020. Toward end-to-end, full-stack 6G terahertz networks. *IEEE Communications Magazine* 58, 11 (2020), 48–54.

[14] S. Redner. 2001. *A Guide to first-passage processes*. Cambridge University Press.

[15] Ryszard Syski. 1992. *Passage times for Markov chains*. Vol. 1. Ios Press.

[16] Yunchou Xing and Theodore S Rappaport. 2021. Propagation Measurements and Path Loss Models for sub-THz in Urban Microcells. *arXiv preprint arXiv:2103.01151* (2021).

[17] Yunchou Xing, Theodore S Rappaport, and Amitava Ghosh. 2021. Millimeter Wave and sub-THz Indoor Radio Propagation Channel Measurements, Models, and Comparisons in an Office Environment. *arXiv preprint arXiv:2103.00385* (2021).

[18] Ping Yang, Yue Xiao, Ming Xiao, and Shaoqian Li. 2019. 6G wireless communications: Vision and potential techniques. *IEEE Network* 33, 4 (2019), 70–75.